Sharpness and intensity modulation of the metal-insulator transition in ultrathin VO_2 films by interfacial structure manipulation

Ryan McGee,[1] Ankur Goswami,[1,*] Soupitak Pal,[2] Kalvin Schofield,[1] Syed Asad Manzoor Bukhari,[1] and Thomas Thundat[1,3,†]

[1]*Department of Chemical and Materials Engineering, University of Alberta, Edmonton, T6G 1H9, Canada*

[2]*Department of Chemical Engineering, University of California, 93106 Santa Barbara, California, USA*

[3]*Department of Chemical and Biological Engineering, University at Buffalo, The State University of New York, Buffalo, New York 14260, USA*

(Received 23 November 2017; published 27 March 2018)

Vanadium dioxide (VO_2) undergoes a structural transformation from monoclinic (insulator) to tetragonal (metallic) upon heating above 340 K, accompanied by abrupt changes to its electronic, optical, and mechanical properties. Not only is this transition scientifically intriguing, but there are also numerous applications in sensing, memory, and optoelectronics. Here we investigate the effect different substrates and the processing conditions have on the characteristics metal-insulator transition (MIT), and how the properties can be tuned for specific applications. VO_2 thin films were grown on *c*-plane sapphire (0001) and p-type silicon ⟨100⟩ by pulsed laser deposition. High-resolution x-ray diffraction along with transmission electron microscopy reveals textured epitaxial growth on sapphire by domain-matching epitaxy, while the presence of a native oxide layer on silicon prevented any preferential growth resulting in a polycrystalline film. An orientation relationship of $\langle 001\rangle(010)_{VO_2}\|\langle 1\bar{1}00\rangle(0001)_{Al_2O_3}$ was established for VO_2 grown on sapphire, while no such relationship was found for VO_2 grown on silicon. Surface-energy minimization is the driving force behind grain growth, as the lowest energy VO_2 plane grew on silicon, while on sapphire the desire for epitaxial growth was dominant. Polycrystallinity of films grown on silicon caused a weaker and less prominent MIT than observed on sapphire, whose MIT was higher in magnitude and steeper in slope. The position of the MIT was shown to depend on the competing effects of misfit strain and grain growth. Higher deposition temperatures caused an increase in the MIT, while compressive strain resulted in a decreased MIT.

DOI: 10.1103/PhysRevMaterials.2.034605

I. INTRODUCTION

A discussion on the paper "Semiconductors with partially and with completely filled $_3d$-lattice bands," authored by de Boer and Verwey, sparked significant interest in transition-metal oxides [1]. Conventional band theory at the time predicted NiO and other transition-metal oxides to behave as conductors; however, this is not the case. Proposed by Mott and Peierls in their discussion of de Boer and Verwey's paper, and theoretically described by Hubbard, this behavior can be attributed to strongly correlated *d*-orbital electrons [2,3]. Although described by Ashcroft and Mermin as a "highly oversimplified model" [4], the Hubbard model has been used to understand several anomalous behaviors including the metal-insulator transition, antiferromagnetism, and superconductivity [5]. The metal-insulator transition (MIT) in transition-metal oxides is driven by the electron correlation effects previously mentioned and is manifested by an incredible change in resistance, on the order of five to ten orders of magnitude [6,7]. This transition is observed in vanadium dioxide (VO_2) at a near room temperature of $T_c = 340$ K for the bulk material.

VO_2 undergoes what is described as a first-order phase transition at T_c from a monoclinic (M1) insulating phase (space group $P2_1/c$) below T_c to a rutile (R) metallic phase (space group $P4_2/mnm$) above T_c [6,8,9]. The transition causes a dimerization of alternating V atoms resulting in two different V-V bond lengths and tilting of these dimers with respect to the *c* axis. The low-temperature phase shows an indirect band gap of 0.6 eV and a large negative temperature coefficient of resistance (TCR) [10,11]. Upon heating past T_c, there is a remarkable increase in conductivity as the lattice transforms into the metallic phase.

These unique properties have resulted in the application of VO_2 thin films towards uncooled microbolometers [12,13], nonvolatile memory [14,15], thermal, optical, and electronic switching [16–18], microcantilevers [19], smart windows [20–22], memristors [23], gas sensors [24], and strain sensors [25]. Although VO_2 has shown promising properties for such a wide range of applications, the deposition of pure phase VO_2 thin films is difficult due to a narrow thermodynamic stability range and a large number of stable and metastable oxide phases such as VO, V_2O_3, V_2O_5, V_nO_{2n-1}, and V_nO_{2n+1} [26]. The characteristics of the MIT have been shown to depend on grain size, interfacial strain, and film thickness, which are strongly influenced by temperature and substrate choice [27–35].

Pulsed laser deposition (PLD) offers an excellent opportunity to study the MIT of VO_2 due to its ability to stoichiometrically transfer target material directly to the substrate. The magnitude of both the hysteresis width and resistance change of the temperature-driven MIT of VO_2 thin films, as well as a shift in the transition temperature, can vary drastically between films deposited on different substrates, or under different conditions

*agoswami@ualberta.ca

†thundat@ualberta.ca

[29,30,33]. By controlling the microstructural properties of the deposited film, the nature of the MIT can be controllably engineered for the desired application. However, in order to exploit the remarkable optical, mechanical and electronic versatility of VO_2, a strong understanding of the film-substrate interface is crucial for a seamless integration into existing micro- and nanofabrication processes. Unfortunately, there has been little work carried out investigating the effect substrate choice and temperature has on the quality of both the crystal structure and MIT of PLD produced VO_2 thin films.

Recently, Marvel *et al.* have reported VO_2 deposition on Si, sapphire, and glass by PLD, sputtering, and electron-beam (e-beam) evaporation; however, the samples did not exhibit any phase transformation without postannealing [30]. However, there was not a significant difference in the MIT temperature or hysteresis characteristics with annealing times less than 90 minutes. Lee *et al.* have reported on the fabrication of several VO_2 polymorphs on several different perovskite substrates, but with little emphasis on the growth condition [36]. Yang *et al.* have reported on the growth of textured VO_2 thin films on heavily doped n^+-Ge (100) and n^+-Si (100) using rf sputtering; however, the reported MIT was underwhelming, and little was done to elucidate strain effect on the MIT [37].

Here we present an investigation into how the choice of substrate and deposition temperature affects the growth behavior and MIT of VO_2 thin films deposited by PLD without postannealing. We investigated how the choice of substrate impacts the texture of the film, phase stability, and the characteristics of the MIT. We studied the simultaneous effect of both deposition temperature and lattice misfit, which provides a new outlook on the modulation of the metal-insulator transition. In this work we report on the modulation of the MIT of VO_2 by elucidating the competing effects that arise between interfacial strain and grain growth by selecting different substrates and growth temperatures simultaneously. While it is known that grain growth will increase the transition temperature, and that compressive stress will reduce the transition temperature, how these two effects combine is not something that has been presented before, and this work attempts to uncover the competing effects of both. Substrate choice imparts a significant impact towards the film-growth mode, as factors such as crystal structure, wettability, and surface energy vary significantly between substrates [38]. Surface-energy minimization is shown to be the major driving force behind film growth, as we investigate how interfacial strain impacts the growth mode. Cubic p-type Si ⟨100⟩ and trigonal *c*-plane sapphire (0001) were chosen as model substrates for deposition of VO_2.

We show that interfacial strain, as a result of the temperature and substrate, significantly impacts the MIT temperature and characteristics. Epitaxial growth of VO_2 on sapphire substrates is achieved through a process called domain-matching epitaxy, which is not observed on silicon. Through cross-sectional transmission electron microscopy, we show that textured growth is inhibited on silicon due to a thin native oxide layer, which brings a disordered amorphous barrier between VO_2 and crystalline silicon. This oxide layer has large ramifications on the growth mode, because the surface energy is significantly lower than pristine silicon, thereby enabling an island-type growth mode as a means to reduce the overall energy. We have monitored the resistance of VO_2 films as a function of temperature in order to quantify the influence that growth parameters have on the MIT. We show that we are able to control the growth of VO_2 thin films by selection of both the substrate and deposition temperatures, and as a result we are able to modulate the behavior of the MIT.

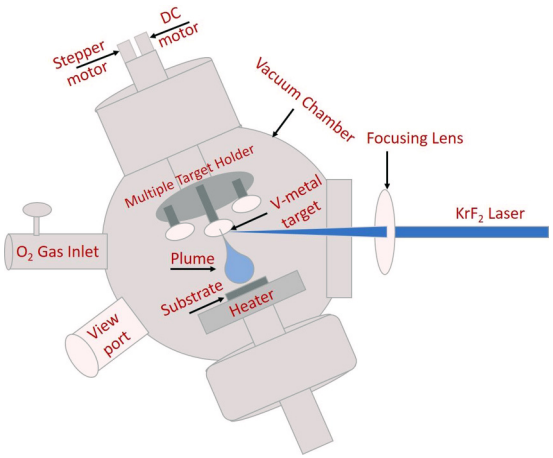

FIG. 1. Schematic of PLD experimental setup, including the laser path and the PLD chamber.

II. EXPERIMENTAL

A. Materials synthesis

VO_2 films were deposited via PLD in an oxygen atmosphere (99.993% purity, Praxair) by using a vanadium metal (99.9% purity, American Elements) circular disk target. A schematic of the setup can be seen in Fig. 1. The target and the substrate are both contained inside a PLD chamber (Excel Instruments, Mumbai, India), with the substrate temperature maintained at one of four temperatures chosen for deposition. The distance between the target and substrate for all experiments was 31 mm. The oxygen pressure inside the chamber is maintained at 100 mTorr throughout the entire deposition. Laser pulses with a 20 ns pulse width from a krypton fluoride (KrF, $\lambda =$ 248 nm) excimer laser (Coherent, GmbH) were directed at the target with a repetition rate of 10 Hz. The laser has a spot size of 1 mm × 3 mm at the target and is maintained at a constant energy density of 2.6 J/cm^2. The deposition time was 15 minutes onto p-type silicon ⟨100⟩ and *c*-cut sapphire (0001) substrates. Deposition parameters were investigated and optimized in our previous work [29]. Prior to deposition the substrates were cleaned with piranha, followed by sonication in milli-Q water, ethanol rinsing, and drying with nitrogen. The chamber pressure was evacuated below 1×10^{-5} torr before the introduction of oxygen. A total of eight films were produced (four for each substrate) and the deposition parameters for each are listed in Table I. Our previous work proved that temperature has a negligible effect on film thickness, and measurements by atomic force microscopy (AFM) and transmission electron microscopy (TEM) confirmed the films were 20–25 nm (see Table T2 in the supplementary material at for the film thickness [39]) [29]. Electrical contacts of Ti/Au (20 nm/80 nm) were deposited onto the film via electron-beam evaporation.

TABLE I. Deposition conditions for each deposited film. The gas pressure (100 mTorr), target-substrate distance (31 mm), and laser fluence (2.6 J/cm^2) were consistent for all experiments.

Sample ID	Substrate	Temperature (°C)	Phase formed
V-SAP-400	*c*-sapphire (0001)	400	VO_2 (M1)
V-SAP-500	*c*-sapphire (0001)	500	VO_2 (A)
V-SAP-550	*c*-sapphire (0001)	550	VO_2 (M1)
V-SAP-600	*c*-sapphire (0001)	600	VO_2 (M1)
V-Si-400	p-Si ⟨100⟩	400	VO_2 (mixed)
V-Si-500	p-Si ⟨100⟩	500	VO_2 (A)
V-Si-550	p-Si ⟨100⟩	550	VO_2 (M1)
V-Si-600	p-Si ⟨100⟩	600	VO_2 (M1)

B. Characterization

1. X-ray diffraction

Thin-film samples were characterized by x-ray diffraction (Rigaku XRD Ultima IV) operating under glancing-angle mode with a 0.5° incident angle and conventional Bragg–Brentano geometries. Such a low incident angle was necessary to eliminate any background signal present from the substrate due to the ultrathin nature of the films. 2θ scanning identified the peak locations; however, due to the close proximity of (020) and (002) peaks, off-axis ϕ scanning was required to properly index the peaks.

2. Surface analysis by atomic force microscopy

A Dimension Fast Scan Atomic Force Microscope (Bruker Nanoscience division, Santa Barbara, CA, USA) was used to measure the surface topography of the films. Commercially available Pt-Ir coated conductive probes (SCM-PIT) with a spring constant of 2.5 N/m and a resonant frequency of 65 kHz were used for obtaining surface topography. The roughness of the samples were determined using nanoscope analysis software from Bruker.

3. Transmission electron microscopy

The film-substrate interface was investigated by transmission electron microscopy (TEM; Titan, FEI, the Netherlands) operated at 300 kV. TEM foils of less than 100 nm thickness were prepared by focused ion beam (FIB) machining (Hellios 600, FEI, The Netherlands), followed by liftoff. Film thickness measurements and diffraction analyses were carried out to determine the crystallinity through selected area diffraction pattern (SAED) and fast fourier transform (FFT) using Digital Micrograph software (Gatan Inc.).

4. Measurement of metal-insulator transition

Temperature-dependant resistance measurements were performed by using a Keithley 2450 source-measure unit (SMU) and the inbuilt Kickstart software in a two-probe configuration. A Signatone 1160 series probe station with a heated chuck connected with the multimeter was used to determine the resistance of the deposited films, which were heated from 5 to 110 °C with 2 °C steps and a 3 minute equilibration time for each step. Both heating and cooling cycles were monitored with the same intervals to probe the hysteretic properties of the MIT. Using a collinear four-point probe configuration on the 2450 SMU, *I*-*V* characteristics for the thin films were collected to determine resistivity.

III. RESULTS AND DISCUSSION

A. X-ray diffraction phase analysis

XRD of the VO_2 thin films revealed that highly textured growth is possible on sapphire (0001) substrates. Figures 2(a) and 2(b) illustrate the resultant x-ray spectra from 2θ scanning of VO_2 films grown at different temperatures on sapphire and silicon. VO_2 grown on sapphire [Fig. 2(a)] presented a unique case where highly textured films were observed for multiple growth temperatures, with one such film grown at 400 °C, which is far below the optimized growth conditions previously observed for VO_2 [29]. There is strong evidence for epitaxial growth of VO_2 films on sapphire at 400, 550, and 600 °C deposition temperatures, as the films show diffraction peaks from the (020) plane at 39.7° and 39.5° and the (004) planes at 85.1° and 85.4°, respectively. The peaks that appear at 41.35° and 90.4° correspond to the (006) and (0012) planes of the substrate, respectively. VO_2 deposited at 500 °C appeared as the (A) phase (JCPDS #82-1074), which is a metastable polymorph of VO_2.

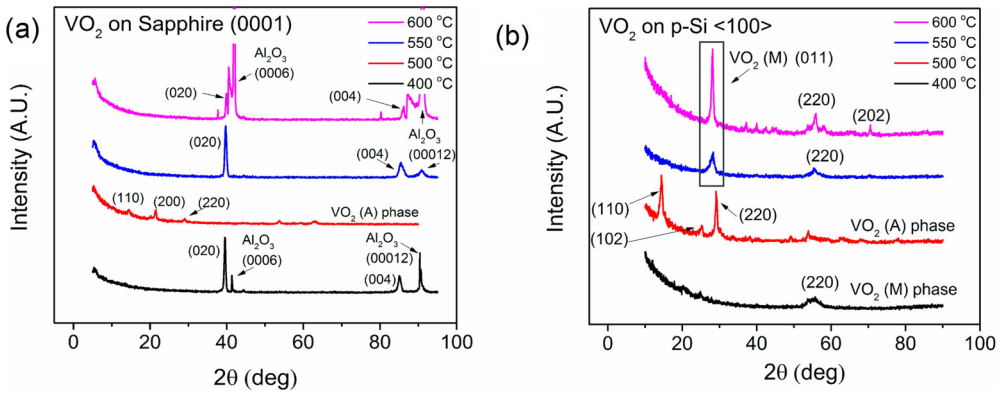

FIG. 2. (a) XRD spectra of VO_2 films deposited on (a) sapphire (0001) and (b) *p*-type Si ⟨100⟩ substrates. The films grown on sapphire showed a highly oriented structure with only the (020) and (004) peaks present, while on silicon a much more polycrystalline structure was observed.

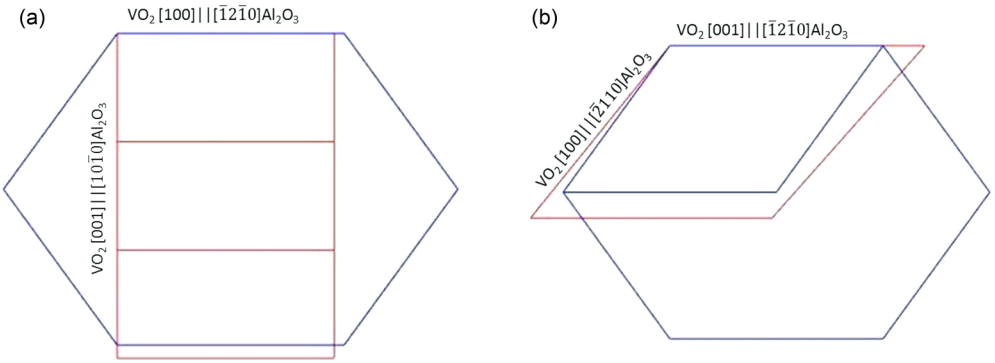

FIG. 3. Schematic of the proposed DME of VO_2 (red) on sapphire (blue) at (a) deposition temperature where VO_2 is present in its tetragonal form and (b) room temperature where the monoclinic phase is present and the c and a axes have flipped.

The appearance of singular peaks for sapphire samples allude to a sort of epitaxial growth behavior. However, at the deposition temperature, the tetragonal and hexagonal crystal systems do not offer an ideal match. The fourfold symmetry of VO_2 (R) does not align nicely with the sixfold symmetry seen in sapphire. Additionally, the c parameter of VO_2 (R) results in an absurdly high lattice mismatch with the sapphire a parameter. It has been proposed by Narayan that an additional type of epitaxial growth is possible, which is unlike lattice-matching epitaxy (LME), and has been called "domain-matching epitaxy" (DME) [40]. DME results when integer multiples of the epilayer matches with integer multiples of the substrate domains, observed in our $(020)_{VO_2}\|(0001)_{Al_2O_3}$ system, shown schematically in Fig. 3. What we have discovered is that the (020) VO_2 plane domain matches the (0001) plane of sapphire if VO_2 is present as tetragonal and monoclinic (accounting for the switching of the a and c axes). The difference between the two scenarios is just the ratio of VO_2 : α-Al_2O_3 domains. During deposition VO_2 is present as rutile and the (020) plane is rectangular with side lengths of $c = 2.86$ Å and $a = 4.55$ Å, with the [001] and [100] directions of VO_2 aligned along the [$\bar{1}2\bar{1}0$] and [$10\bar{1}0$] directions of sapphire, respectively. Upon cooling to room temperature, the orientation of the (020) plane tilts and the a and c axes flip, as per the nature of the transition. The (020) plane is now oriented on the substrate with the [001] and [100] directions of VO_2 aligned with the [$\bar{1}2\bar{1}0$] and [$\bar{2}110$] directions of sapphire, respectively. In the former case, the DME relationship is $3VO_2$: 1 sapphire along the c direction of VO_2, and a 1 : 1 ratio along the VO_2 a direction, resulting is a mismatch of 4.3% in both cases. For the latter case, for VO_2 to sapphire ratios of 7 : 8 and 4 : 5 along the VO_2 c and a directions, respectively, lattice mismatch is reduced to 0.89% and 3.1%. Without the possibility of DME growth, epitaxial films in this system would be highly unlikely because the lattice mismatch is too great to overcome. DME enables pseudomorphic growth of high-quality films, which would be otherwise impossible, by matching domains rather than individual lattice sites, thereby reducing mismatch [41].

The primary peaks of VO_2 located at 39.55°, 39.7°, and 39.9° for V-SAP-400, V-SAP-550, and V-SAP-600, respectively, were attributed to the (020) reflection, and not (002) which also appears at the 2θ value. This was solved by performing off-axis ϕ scanning of the ($\bar{2}11$) reflection of VO_2 which has ϕ angles of 57.635° and 90.297° with the (020) and the (200) reflections, respectively. Figure 4 shows the resultant profile of the off-axis scans, with the appearance of six peaks between the ($\bar{2}11$) and (020) system, and none between ($\bar{2}11$) and (002) (Fig. 4, inset).

XRD spectra for VO_2 films grown on silicon substrates showed a more random orientation than those grown on sapphire, indicated by the presence of multiple diffraction peaks. At 400 °C, there are dim peaks that correspond to VO_2 (M) phase, but the crystallinity was weak. Again, at 500 °C the deposition resulted in the (A) phase polymorph, also observed for VO_2 deposited on sapphire. When deposited at 600 °C, the XRD spectrum revealed the presence of a polycrystalline VO_2 thin film with primary 2θ peaks at 28.15°, 37.2°, and 55.8°, which correspond to the (011), (200), and the (220) planes, respectively. However, it is apparent that VO_2 grows with a higher preference as (011) when compared with the intensity of other peaks. A common theme observed for films deposited on both substrates is a deviation from the ideal peak location. Deviations of the diffraction peaks can be affected by many things, among them is lattice mismatch. Lattice mismatch is realized as an in-plane tensile or compressive strain which is capable of impacting the d spacing, as observed here. The

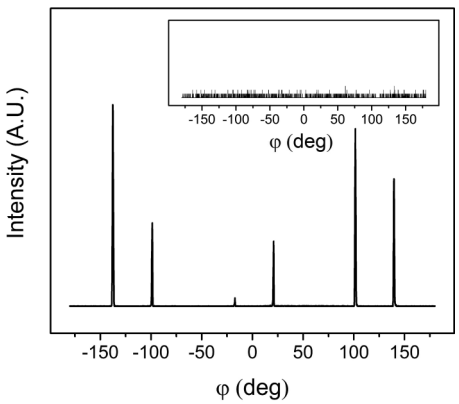

FIG. 4. Off-axis scanning of V-SAP-550 of the ($\bar{2}11$) reflection at $2\theta = 36.972°$ with ψ angle of 57.635° between ($\bar{2}11$) and (020) reflections. Inset shows the absence of the ($\bar{2}11$) reflection at $2\theta = 36.972°$ and ψ of 90.297°, the angle between the ($\bar{2}11$) and (002) planes.

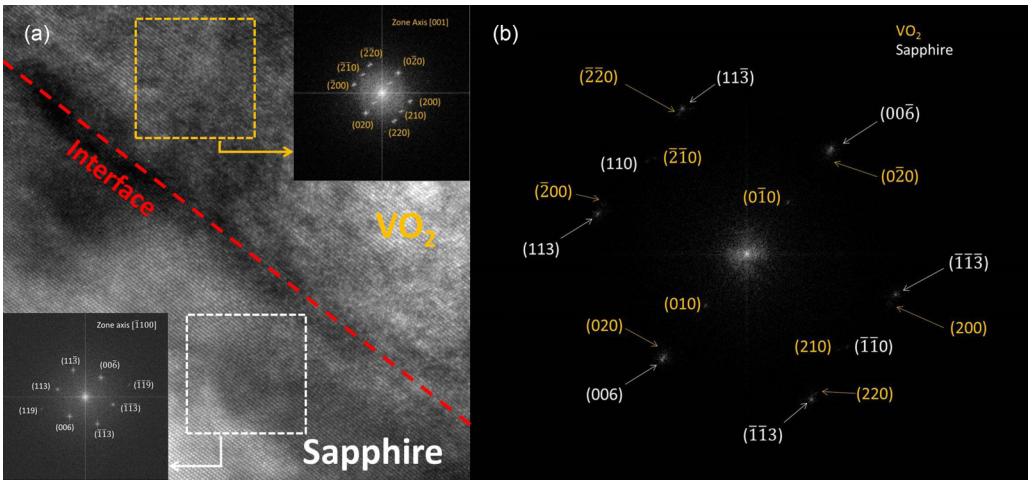

FIG. 5. (a) High-resolution TEM image of the VO_2/sapphire cross section V-SAP-600 film. Inset in the bottom-left corner shows the diffraction pattern of sapphire. The top-right corner shows the diffraction pattern of the VO_2 film (b) FFT of the VO_2/sapphire interface. The diffraction spots in panel (b) correspond to the $[\bar{1}100]$ and [001] zones of sapphire and VO_2, respectively.

lattice misfit parameter f_m can be calculated by

$$f_m = \frac{a_f - a_s}{a_s}, \tag{1}$$

where a_f and a_s are the film and substrate lattice constants, respectively. The high sensitivity of XRD enables detection of subtle changes in the lattice plane d spacing, which was manifested as a shift in 2θ values. This change can be mathematically determined by the Bragg equation, which relates the interplanar spacing to the angle of the diffracted beam as [42]

$$2d \sin\theta = n\lambda, \tag{2}$$

where d is the spacing between lattice planes, θ is the angle of the diffracted beam, n is a positive integer, and λ is the wavelength of the incoming x-ray beam (here the source is Cu $K\alpha$, $\lambda = 0.15418$ nm). Lattice mismatch results in a combination of in-plane strain and the formation of strain-relaxing misfit dislocations, both of which have been shown to profoundly impact the characteristics of the MIT [37].

Mentioned briefly above was the deposition of VO_2 (A) phase at 500 °C, regardless of substrate. The (A) phase differs from the low-temperature (M1) phase both structurally and electronically. Debate over the exact structure of the (A) phase persists, although it is accepted to be of the tetragonal crystal system at room temperature, and does not exhibit any phase transition at the T_c observed for VO_2 (M1) films. On sapphire, the VO_2 (A) phase manifested as the appearance of diffraction peaks at 2θ values of 14.5°, 21.5°, and 29.0°, which correspond to the (110), (200), and (220) planes, respectively [see Fig. S3 in the supplementary material at for a detailed explanation of VO_2 (A) grown on sapphire [39]]. VO_2 grown on Si results in the appearance of diffraction peaks at 2θ values of 14.4°, 25.25°, and 29.1° for the (110), (102), and (220) planes, respectively. Evidence of peaks shifting from their ideal values was present in both film-substrate systems; however, due to the difference in both the lattice constants and crystal structure of Si and sapphire, the peak shifts were not equivalent for the two different films. This further confirms the suspicion that the peak shift was a result of strain imparted by lattice mismatch, as each unique film-substrate interface will result in varying degrees of strain. The appearance of VO_2 (A) at 500 °C is commensurate with our previous parametric study of PLD of VO_2 thin films on SiO_2 substrates which also showed the formation of VO_2 (A) at 500 °C [29]. The consistent formation of VO_2 (A) at 500 °C regardless of substrate indicates the presence of a local minima in the free-energy framework of VO_2, which appears independent of substrate-film-related phenomena such as interfacial strain and crystallinity. It has been shown before that, above a certain temperature, VO_2 (A) will decompose into VO_2 (M1), which is why we see the (A) phase disappear at 550 °C [36]. Additionally, it has been shown that the formation energy for the (A) phase is much higher than that of the M1 phase, and this would explain why we do not see it form at the lower temperature [43].

B. Cross-sectional transmission electron microscopy analysis

The substrate-film interface has been characterized by using cross-sectional high-resolution transmission electron microscopy (HRTEM) on the V-SAP-600 and V-Si-600 films. Figure 5(a) shows the cross-sectional HRTEM of the sapphire/VO_2 interface displaying epitaxial growth of the VO_2 phase on the sapphire substrate. The FFT pattern captured from the film-substrate conjugate is shown in Fig. 5(b). Orientation of the sapphire substrate parallel to the beam direction is $\langle 1\bar{1}00\rangle$, whereas the orientation of the film is $\langle 001\rangle$. The (006) planes of alumina and the (020) planes of VO_2 are parallel to the interface, where the normal directions to those planes, $\langle 0001\rangle$ and $\langle 010\rangle$, respectively, are also parallel to each other. HRTEM analysis also supports the observed growth of $\langle 020\rangle$ texture of VO_2 on sapphire. Comparing the lattice parameter values of monoclinic VO_2, given in Table II, we can further comment that the growth along the $\langle 010\rangle$ direction of monoclinic VO_2 will be more feasible. Growth of VO_2 on silicon does not select any special orientation relationship but rather it grows in a nontextured manner following the ideal powder diffraction pattern of VO_2, as shown in Fig. 2(b). The cross-sectional HRTEM image of the V-Si-600 sample and the corresponding

TABLE II. Lattice parameters (Å) for VO_2, sapphire, and silicon.

Substrate	System	a	b	c	β	Space Group
c-sapphire (0001)	Rhombohedral	4.76	4.76	12.99		$R\bar{3}c$
p-Si ⟨100⟩	Cubic	5.43	5.43	5.43		$Fd\bar{3}$m
VO_2 (R)	Tetragonal	4.56	4.56	2.86		$P4_2/mnm$
VO_2 (M1)	Monoclinic	5.75	4.54	5.38	122.65	$P2_1$/c
VO_2 (A)	Tetragonal	8.48	8.48	7.62		$P4_2/ncm$

FFT pattern show that the film, marked in Fig. 6(a), does not exhibit any orientation relationship with the substrate. Furthermore, a thin native oxide layer of ∼3 nm is clearly visible at the film-substrate interface.

C. Surface characterization by atomic force microscopy

We used AFM to investigate the physical nature of the deposited VO_2 thin films. Surface roughness was found to depend significantly on the temperature and the substrate, although the trend was not very straightforward. The surface roughness of the virgin substrates and the deposited films are presented in Table III. Immediately it is apparent that VO_2 (A) resulted in the roughest surface, regardless of substrate, and that roughness responded to temperature differently for each substrate. Surface roughness is highly affected by the growth mode, of which there are three main methods: Frank-van der Merwe (FM, layer by layer), Volmer–Weber (VW, island growth), and Stranski–Krastanov (SK, layer plus island) [44]. The determination of the growth mode depends upon the surface energies of the film, substrate, and the film-substrate interface (γ_f, γ_s, and γ_i) investigated. The driving force between which growth mode is observed is a minimization of the overall surface energy of the system, which may be affected by surface diffusion. FM growth will occur if $\gamma_f + \gamma_i \leqslant \gamma_s$ and VW growth will occur if $\gamma_f > \gamma_s$. The surface energy of the (0001) surface ranges between 2.03 and 12.85 J/m^2, with the value for VO_2 being an order of magnitude lower, indicating a strong likelihood to see FM growth [45]. On the other hand, the native oxide on Si wafers has a much lower surface energy, ranging from 0.164 to 0.237 J/m^2 which is of the same magnitude as that of (110) VO_2 [46,47].

Surface-energy minimization is why we see the growth of the (011) plane on the Si substrate, because this is the lowest-energy plane for VO_2. Surface roughness does not vary much for the Si/VO_2 (M1) system, likely due to this fact. The slight decrease in the roughness as temperature increases can be attributed to an increase in surface diffusion of adatoms, allowing for greater coverage of the surface. On the other hand, the sapphire/VO_2 (M1) system showed a significant decrease in surface roughness when temperature is increased. AFM micrographs from the two samples grown at 600 °C are shown in Fig. 7 . For the AFM images of the remaining six samples and the bare substrates, refer to Figs. S1 and S2 in the supplementary material [39]. From XRD and TEM we showed that VO_2 grows in a textured polycrystalline structure, which means that the lowest-energy plane [i.e., (011)] did not grow on sapphire. However, the appearance of textured epitaxial growth, as observed for VO_2 on sapphire, indicates a minimization of the interfacial surface energy by growing in preferential orientations. By minimizing the interfacial surface energy, we still satisfy the equation for FM growth mode; $\gamma_f + \gamma_i \leqslant \gamma_s$. The decrease in roughness as temperature increased can also be attributed to the increase in surface mobility of adatoms, as seen on Si.

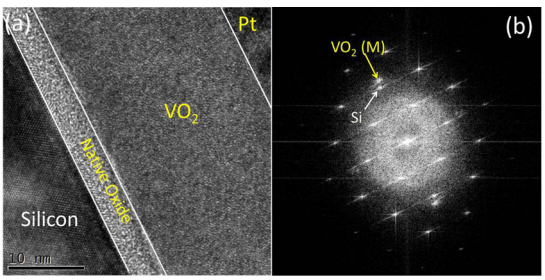

FIG. 6. (a) High-resolution TEM image of the VO_2/silicon interface taken from V-Si-600 and (b) the corresponding FFT pattern of the entire image.

D. Metal-insulator transition

1. Temperature vs resistance measurements

We investigated the substrate-dependant nature of the MIT of VO_2 thin films by monitoring the variation in electrical resistance as a function of substrate temperature. We found that VO_2 grown on sapphire [Fig. 8(a)] resulted in the sharpest MIT, with the highest magnitude and lowest hysteresis. The films grown on silicon (Fig. 8) showed a narrow hysteresis as well, but suffered from a low-magnitude MIT. Compared to our previous results probing the MIT for VO_2 grown on SiO_2, VO_2 grown on sapphire and silicon had a much narrower hysteresis width, with similar transition magnitudes.

Figure 8(a) shows the temperature vs resistance curves for the heating-cooling cycle of VO_2 on sapphire. Of the four films grown on sapphire, only one (V-SAP-500) did not show any evidence of a MIT, because the VO_2 (A) phase does not

TABLE III. Surface roughness for VO_2 thin films grown on Si and sapphire.

Sample ID	Surface roughness (nm)			
	400 °C	500 °C	550 °C	600 °C
VO_2/sapphire[a]	2.83	3.14	0.74	0.51
VO_2/Si[b]	2.0	3.2	1.74	1.9

[a]Bare sapphire roughness was 0.14 nm.
[b]Bare silicon roughness was 0.15 nm.

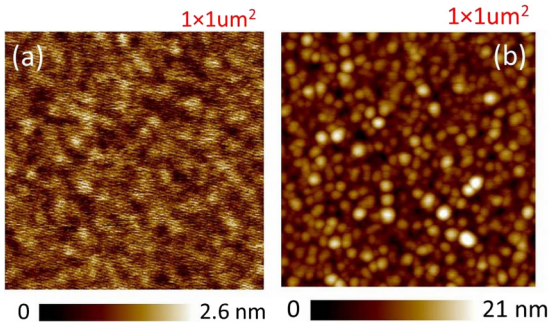

FIG. 7. AFM images showing the surface profile of (a) VO_2 on sapphire (V-SAP-600) and (b) silicon (V-Si-600). The rms roughness values in Table III were computed from these images.

undergo such a transition in the temperature range studied. The remaining three films all demonstrated evidence of the MIT with varying properties as listed in Table IV. V-SAP-400 and V-SAP-600 both demonstrated just over three orders of magnitude change in resistance, with V-SAP-400 having a much larger hysteresis width. Additionally, V-SAP-400 and V-SAP-600 displayed sharp transitions from both metal-insulator and insulator-metal, with values exceeding 10^4 Ω cm/°C, which makes for an attractive choice for ultrafast-switching applications [16]. On the contrary, V-SAP-550 does not show such a large magnitude or steep transition, but does have a minimal hysteresis width throughout the entire heat-cool cycle, which is an attractive property in itself.

As shown previously by XRD, VO_2 grown on silicon substrates produced the (M1) phase for deposition temperatures of 550 and 600 °C, and this is apparent from the temperature vs resistance measurements shown in Fig. 8(b). Of the four films, only three formed VO_2, and of those only two (V-Si-550 and V-Si-600) displayed a transition, while the other (V-Si-500) did not. V-Si-500 was present as VO_2 (A) phase, so no transition was expected as reported previously [29,36]. V-Si-600 showed a very narrow MIT hysteresis width, with a transition magnitude of nearly two orders. V-Si-550 showed similar hysteresis and magnitude to that of V-Si-600, but the transition occurred at a much lower temperature. The MIT for both of these films was found to have a much gentler

TABLE IV. Magnitude (Ω), hysteresis width (Δ °C), and position (°C) of the metal-insulator transition for VO_2 grown on *c* sapphire (0001).

Sample ID	Magnitude	Hysteresis width	Position
V-SAP-400	$10^{3.4}$	10.8	51.9
V-SAP-550	$10^{2.7}$	2.7	47.8
V-SAP-600	$10^{3.3}$	3.6	51

slope as compared with VO_2 grown on sapphire. Summarized in Table V, the MIT properties of VO_2 thin films grown on silicon were found to differ significantly from those grown on sapphire. In addition to a much lower magnitude compared with VO_2 on sapphire, the MIT of the films grown on silicon were not nearly as pronounced, i.e., their slope was much less than on sapphire. Resistivity measurements were conducted at temperatures below (room temp ∼20 °C) and above (100 °C) to see the effect of substrate and temperature. Presented in Table T1 in the supplementary material [39], resistivity is shown to decrease as temperature increases, while between substrates, resistivity of VO_2 is shown to vary significantly more for films grown on sapphire. Increased temperature has been shown to result in larger grains, thereby decreasing the grain-boundary density, which should (and does) result in a lower resistivity.

2. *Correlation between structure and metal-insulator transition of* VO_2

It has been shown that interfacial strain, which may arise from lattice mismatch, has a profound effect on the MIT. Aetukuri *et al.* showed the ability to manipulate the MIT in VO_2 by controlling orbital occupancy by means of epitaxial strain modulation [48]. Nagashima *et al.* have shown that the *c*-axis length in VO_2 thin films influences the position and slope of the MIT [49,50]. With deposition occurring at 600 °C, VO_2 was present as the tetragonal phase, which produces a small lattice misfit strain on sapphire (−4.4%) as opposed to a much larger value when the substrate is silicon (−16.2%). However, upon cooling below the transition temperature, the tetragonal phase transforms to the monoclinic phase, defined by a flipping of the *a* and *c* axes, coupled with dimerization and

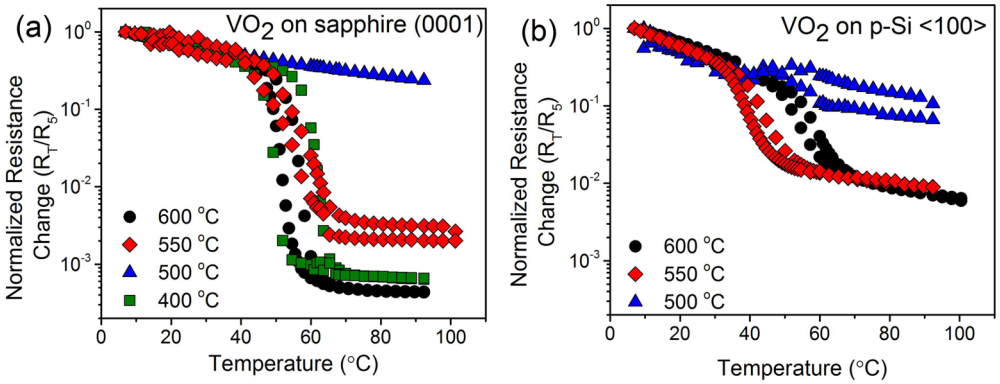

FIG. 8. Resistance as a function of temperature for VO_2 thin films grown on (a) sapphire and (b) silicon substrates. Common to both is no transition present for the films grown at 500 °C, and a sharp transition for films grown at 550 and 600 °C. On Si, VO_2 did not deposit at 400 °C and therefore no measurement was taken.

TABLE V. Magnitude (Ω), hysteresis width (Δ °C), and position (°C) of the metal-insulator transition VO_2 grown on p-Si ⟨100⟩.

Sample ID	Magnitude	Hysteresis width	Position
V-Si-550	$>10^{1.5}$	4.5	37.05
V-Si-600	$>10^{1.5}$	5.4	51.9

tilting of alternating vanadium atoms along the monoclinic *a* axis (resulting in an elongation along this axis by 1%).

The nature of the strain (compressive or tensile) can be determined for each system by looking at the *d*-spacing equation for each system. Here, we deposited both the (A) and (M1) phase, which are tetragonal and monoclinic, respectively. The *d*-spacing for each crystal system is measured as the reciprocal of length of the reciprocal-lattice vector [51]. For the tetragonal system,

$$\frac{1}{d_{hkl}^2} = \frac{h^2 + k^2}{a^2} + \frac{l^2}{c^2}, \tag{3}$$

and for the monoclinic system,

$$\frac{1}{d_{hkl}^2} = \frac{h^2}{a^2 \sin^2\beta} + \frac{k^2}{b^2} + \frac{l^2}{c^2 \sin^2\beta} + \frac{2hl\cos\beta}{ac\sin^2\beta}, \tag{4}$$

where a, b, and c are the lattice parameters, β is the angle between the a and c axes, and h, k, and l are the the Miller indices (hkl). Lattice parameters for the substrates and VO_2 phases can be found in Table II, which have been taken from literature and used to determine theoretical lattice misfit [52–56].

Based on the results from XRD and the values in Table II, we were able to determine the nature of the strain (tensile or compressive) due to the apparent change in the *d* spacing observed. The change in *d* spacing can be used to determine, by using Eqs. (3) and (4), how the lattice parameters are affected by the mismatch. Summarized in Table VI are the theoretical and experimentally determined *d*-spacing values for the primary peaks observed in XRD, and the corresponding strain type.

What is apparent from the table is that not only does the substrate affect the observed *d* spacing, but also the temperature of deposition. For the sapphire/VO_2 (M1) system, an increase in the temperature resulted in a lower value of *d* spacing, with the deviation from the ideal value increasing as well. For the Si/VO_2 (M1) system, the opposite scenario is true, where the *d* spacing increases with temperature, and the *d* spacing becomes closer to the theoretical value. In both cases, however, the strain is seen to be of the same type, as all cases involving VO_2 (M1) resulted in a compressed *d* spacing, with the exception of V-SAP-400. Park *et al.* have shown that a compression results in a lower MIT temperature from monoclinic to rutile, which was observed for all cases of VO_2 (M1) studied herein [57]. This is not the only factor which influences the MIT, as in the sapphire/VO_2 (M1) system the transition temperature fluctuates and does not follow a specific trend. It has been shown that the grain size also influences the MIT temperature, and in our previous work we have shown that deposition temperature has a significant impact on the resultant grain size. Miller and Wang have shown that samples with a higher density of grain boundaries (smaller grain size) offer a greater amount of nucleation sites, resulting in a lower T_c [27]. This is likely the reason we observed the increased transition temperature for sample V-SAP-600, as the competing effects of grain size vs strain had a larger contribution from grain size. On the other hand, V-SAP-400 has a higher transition temperature with a larger density of grains and a tensile strain in the film, showing the opposite competition between strain and grain size. V-SAP-400 has much smaller grain size, which should reduce the T_c, but the tensile stain causes an increase. Here, since T_c is less than the bulk value a larger effect is seen from the reduced grain size.

The primary difference observed between the Si and sapphire system was the presence of multiple diffraction peaks on Si. Considering both substrates were single crystals, one would assume there to be preferential growth for Si as there was for sapphire. However, the clean silicon surface will undoubtedly form a native oxide layer prior to deposition due to exposure to atmospheric oxygen as well as the oxygen in the PLD chamber as also shown in Fig. 6(a). In addition to the oxidation, it has been shown by high-energy ion backscattering techniques that the first few Si layers of the Si-SiO_2 interface are nonregistered, and are their positions are incommensurate with the bulk Si lattice (shifting of up to 1 Å is observed) [58]. This subsurface reconstruction has ramifications on the nature of the oxide layer as well, resulting in the stoichiometric SiO_2 surface layer displaying amorphous behavior, similar to that of thermally grown SiO_2 substrates. Ultimately, rather than depositing on virgin Si substrates, the VO_2 is actually deposited on an amorphous oxide layer, similar to that of the thermal oxide. Due to the nature of this surface reconstruction and oxidation it is not surprising that VO_2 grown on these substrates exhibit a slower transition and a greater degree of polycrystallinity.

TABLE VI. Experimental and theoretical *d* spacing (Å) for the observed lattice planes.

Sample ID	Observed plane	*d* spacing (theoretical)	*d* spacing (actual)	Strain type
V-SAP-400	(020)	2.2689	2.2768	Tensile
V-SAP-500	(200)	4.2415	4.1392	Compressive
V-SAP-550	(020)	2.2689	2.2691	Compressive
V-SAP-600	(020)	2.2689	2.2576	Compressive
V-Si-500	(110)	5.9983	6.1460	Tensile
V-Si-550	(011)	3.2067	3.1620	Compressive
V-Si-600	(011)	3.2067	3.1675	Compressive

IV. CONCLUSION

In this work we deposited VO_2 thin films onto *c*-cut (0001) sapphire and p-type Si ⟨100⟩ by PLD at multiple temperatures to establish any substrate-related influence on the structural and electronic properties of the deposited films. VO_2 on sapphire was shown by TEM and XRD to grow epitaxially, with the (020) plane growing preferentially, whereas on silicon, VO_2 showed a polycrystalline nature, with the appearance of several diffraction peaks. TEM also revealed that a thin (∼2 nm) native oxide layer had formed on the surface, preventing any preferential growth. Surface-roughness measurements showed VO_2 grown on sapphire had a much stronger roughness vs temperature dependance, with a significant decrease in roughness as temperature increased. On silicon, the roughness decreased marginally with increasing temperature, indicating two different mechanisms at play. Surface-energy minimization dictated the growth mode, and therefore the surface roughness, as VO_2 on sapphire was driven to reduce interfacial surface energy (as evidenced by epitaxial growth), while similar surface energies between VO_2 and native SiO_2 show more layer-plus-island growth resulting a rougher film. Roughness decrease as a result of increasing temperature is attributed to grain-boundary migration due to increased diffusion. The characteristics of the metal-insulator transition depended on the temperature and substrate chosen, because VO_2 on sapphire had a much sharper and larger resistance drop at the transition temperature as compared with VO_2 on silicon, which showed a weaker, more gradual change from insulator to metal. Compressive strain pushes the MIT temperature to a lower value, while competing effects from grain growth prevent a large decrease. VO_2 (M1) on Si grows in a much more polycrystalline nature than on sapphire due to the amorphous characteristics of the native oxide overgrowth.

ACKNOWLEDGMENTS

This work was supported by the Canada Excellence Research Chair (CERC) Program (ID: SF0926 and Grant No. RES 0006296). The authors acknowledge the characterization facilities provided by the nanofab at the University of Alberta. Kristi McGuire and Liang Zhou are acknowledged for conducting the temperature-dependant resistance measurements and resistivity measurements.

[1] J. H. de Boer and E. J. W. Verwey, Proc. Phys. Soc. **49**, 59 (1937).
[2] N. F. Mott and R. Peierls, Proc. Phys. Soc. **49**, 72 (1937).
[3] J. Hubbard, Proc. R. Soc. London, Ser. A **276**, 238 (1963).
[4] N. Ashcroft and N. Mermin, *Solid State Physics* (Holt, Rinehart and Winston, New York, 1976).
[5] H. Tasaki, J. Phys.: Condens. Matter **10**, 4353 (1998).
[6] F. J. Morin, Phys. Rev. Lett. **3**, 34 (1959).
[7] N. F. Mott, Rev. Mod. Phys. **40**, 677 (1968).
[8] G. Andersson, C. Parck, U. Ulfvarson, E. Stenhagen, and B. Thorell, Acta Chem. Scand. **10**, 623 (1956).
[9] N. F. Mott and L. Friedman, Philos. Mag. (1798–1977) **30**, 389 (1974).
[10] H. W. Verleur, A. S. Barker, Jr., and C. N. Berglund, Phys. Rev. **172**, 788 (1968).
[11] B. Wang, J. Lai, H. Li, H. Hu, and S. Chen, Infrared Phys. Technol. **57**, 8 (2013).
[12] H. Jerominek, T. D. Pope, M. Renaud, N. R. Swart, F. Picard, M. Lehoux, S. Savard, G. Bilodeau, D. Audet, P. L. Ngo, and Q. C. Nong, in *Proceedings Volume 3061, Infrared Technology and Applications XXIII; (1997), AeroSense '97, 1997*, Orlando, Florida, United States.
[13] R. T. Rajendra Kumar, B. Karunagaran, D. Mangalaraj, Sa K. Narayandass, P. Manoravi, M. Joseph, and V. Gopal, Smart Mater. Struct. **188**, 187 (2003).
[14] L. Pellegrino, N. Manca, T. Kanki, H. Tanaka, M. Biasotti, E. Bellingeri, A. S. Siri, and D. Marré, Adv. Mater. **24**, 2929 (2012).
[15] L. Fan, Y. Chen, Q. Liu, S. Chen, L. Zhu, Q. Meng, B. Wang, Q. Zhang, H. Ren, and C. Zou, ACS Appl. Mater. Interfaces **8**, 32971 (2016).
[16] G. Stefanovich, A. Pergament, and D. Stefanovich, J. Phys.: Condens. Matter **12**, 8837 (2000).
[17] M. Rini, Z. Hao, R. W. Schoenlein, C. Giannetti, F. Parmigiani, S. Fourmaux, J. C. Kieffer, A. Fujimori, M. Onoda, S. Wall, and A. Cavalleri, Appl. Phys. Lett. **92**, 181904 (2008).
[18] A. Gupta, R. Aggarwal, and J. Narayan, MRS Online Proc. Libr. **1174** (2009).
[19] R. McGee, A. Goswami, R. Abraham, S. Bukhari, and T. Thundat, MRS Adv. (2018), doi:10.1557/adv.2018.140.
[20] J. Zhou, Y. Gao, Z. Zhang, H. Luo, C. Cao, Z. Chen, L. Dai, and X. Liu, Sci. Rep. **3**, 3029 (2013).
[21] Y. Ke, I. Balin, N. Wang, Q. Lu, A. Iing, Y. Tok, T. J. White, S. Magdassi, I. Abdulhalim, and Y. Long, ACS Appl. Mater. Interfaces **8**, 33112 (2016).
[22] J. Zhu, Y. Zhou, B. Wang, J. Zheng, S. Ji, H. Yao, H. Luo, and P. Jin, ACS Appl. Mater. Interfaces **7**, 27796 (2015).
[23] S.-H. Bae, S. Lee, H. Koo, L. Lin, B. H. Jo, C. Park, and Z. L. Wang, Adv. Mater. **25**, 5098 (2013).
[24] E. Strelcov, Y. Lilach, and A. Kolmakov, Nano Lett. **9**, 2322 (2009).
[25] B. Hu, Y. Ding, W. Chen, D. Kulkarni, Y. Shen, V. V. Tsukruk, and Z. L. Wang, Adv. Mater. **22**, 5134 (2010).
[26] K. Kosuge, J. Phys. Chem. Solids **28**, 1613 (1967).
[27] M. J. Miller and J. Wang, J. Appl. Phys. **117**, 034307 (2015).
[28] Y. Zhao, J. H. Lee, Y. Zhu, M. Nazari, C. Chen, H. Wang, A. Bernussi, M. Holtz, and Z. Fan, J. Appl. Phys. **111**, 053533 (2012).
[29] R. McGee, A. Goswami, B. Khorshidi, K. Mcguire, K. Schofield, and T. Thundat, Acta Mater. **137**, 12 (2017).
[30] R. E. Marvel, R. R. Harl, V. Craciun, B. R. Rogers, and R. F. Haglund, Acta Mater. **91**, 217 (2015).
[31] L. L. Fan, S. Chen, Z. L. Luo, Q. H. Liu, Y. F. Wu, L. Song, D. X. Ji, P. Wang, W. S. Chu, C. Gao, C. W. Zou, and Z. Y. Wu, Nano Lett. **14**, 4036 (2014).
[32] L. L. Fan, S. Chen, G. M. Liao, Y. L. Chen, H. Ren, and C. W. Zou, J. Phys.: Condens. Matter **28**, 255002 (2016).
[33] T. Yamin, S. Wissberg, H. Cohen, G. Cohen-Taguri, and A. Sharoni, ACS Appl. Mater. Interfaces **8**, 14863 (2016).

[34] Y. Li, S. Ji, Y. Gao, H. Luo, and P. Jin, ACS Appl. Mater. Interfaces **5**, 6603 (2013).
[35] J. Nag, E. A. Payzant, K. L. More, and R. F. Haglund, Appl. Phys. Lett. **98**, 251916 (2011).
[36] S. Lee, I. N. Ivanov, J. K. Keum, and H. N. Lee, Sci. Rep. **6**, 19621 (2016).
[37] Z. Yang, C. Ko, and S. Ramanathan, J. Appl. Phys. **108**, 073708 (2010).
[38] C. V. Thompson, Annu. Rev. Mater. Res. **42**, 399 (2012).
[39] See Supplemental Material at http://link.aps.org/supplemental/10.1103/PhysRevMaterials.2.034605 for additional characterization data of the VO_2 films.
[40] J. Narayan and B. C. Larson, J. Appl. Phys. **93**, 278 (2003).
[41] A. Moatti, R. Sachan, J. Prater, and J. Narayan, ACS Appl. Mater. Interfaces **9**, 24298 (2017).
[42] W. H. Bragg and W. L. Bragg, Proc. R. Soc. London, Ser. A **88**, 428 (1913).
[43] N. Bahlawane and D. Lenoble, Chem. Vap. Deposition **20**, 299 (2014).
[44] H. Brune, in *Surface and Interface Science: Solid-Solid Interfaces and Thin Films*, 1st ed., edited by K. Wandelt (Wiley-VCH Verlag GmbH & Co., Weinheim, Germany, 2014), Chap. 20.
[45] S. Blonksi and S. Garofalini, Surf. Sci. **295**, 263 (1993).
[46] R. G. Frieser, J. Electrochem. Soc. **121**, 669 (1974).
[47] T. A. Mellan and R. Grau-Crespo, J. Chem. Phys. **137**, 154706 (2012).
[48] N. B. Aetukuri, A. X. Gray, M. Drouard, M. Cossale, L. Gao, A. H. Reid, R. Kukreja, H. Ohldag, C. A. Jenkins, E. Arenholz, K. P. Roche, H. A. Durr, M. G. Samant, and S. S. P. Parkin, Nat. Phys. **9**, 661 (2013).
[49] K. Nagashima, T. Yanagida, H. Tanaka, and T. Kawai, J. Appl. Phys. **101**, 026103 (2007).
[50] K. Nagashima, T. Yanagida, H. Tanaka, and T. Kawai, Phys. Rev. B **74**, 172106 (2006).
[51] A. Kelly and K. M. Knowles, in *Crystallography and Crystal Defects* (John Wiley & Sons, Ltd., Chichester, 2012), pp. 469–472.
[52] J. M. Longo and P. Kierkegaard, Acta Chem. Scand. **24**, 420 (1970).
[53] D. B. McWhan, M. Marezio, J. P. Remeika, and P. D. Dernier, Phys. Rev. B **10**, 490 (1974).
[54] M. Oetzel and G. Heger, J. Appl. Crystallogr. **32**, 799 (1999).
[55] M. E. Straumanis, E. Z. Aka, and S. And, J. Appl. Phys. **23**, 330 (1952).
[56] T. Yao, Y. Oka, and N. Yamamoto, J. Solid State Chem. **112**, 196 (1994).
[57] J. H. Park, J. M. Coy, T. S. Kasirga, C. Huang, Z. Fei, S. Hunter, and D. H. Cobden, Nature (London) **500**, 431 (2013).
[58] A. H. Al-Bayati, K. G. Orrman-Rossiter, J. A. Van Den Berg, and D. G. Armour, Surf. Sci. **241**, 91 (1991).